Bias correction for the orientation distribution of slump fold axes: Application to the Cretaceous Izumi basin

Toshiyuki Koyama[a], Atsushi Yamaji[a,*], Katsushi Sato[a]

[a]*Division of Earth and Planetary Sciences, Graduate School of Science, Kyoto University, Kyoto 606-8502, Japan*

Abstract

Linear structures perpendicular to an outcrop surface are easily discovered, but those parallel to the surface are not, giving rise to a biased orientation distribution of the structures. Here, we propose a bias correction method: Statistical inversion was conducted to unbias the distribution of the axes of mesoscale slump folds in the Cretaceous Izumi Group, Japan using the orientation distribution of outcrop surfaces. The observed axes showed a cluster in the SE quadrant. Their unbiased distribution had a girdle pattern with a maximum concentration orientation in the same quadrant, but the unbiased one had a lower peak density than the observed one, and was more girdle-like than the observed one. The maximum concentration axis of the unbiased distribution was roughly perpendicular to the paleocurrents observed in the same area. Therefore, the popular view that the axes of slump folds are perpendicular to paleoslope applies to the folds in the area in a statistical sense. The hypothesis about the vergences of slump folds and paleoslope hold only about a half of the observed slump folds.

Keywords: selection bias, soft sediment deformation, statistical inversion, Bingham distribution

*Corresponding author. Tel.: +81 75 753 4266; fax: +81 75 753 4289.
Email address: yamaji@kueps.kyoto-u.ac.jp (Atsushi Yamaji)

1. Introduction

Observation of the orientation distribution of planar structures such as faults and joints is known to be affected by selection bias (e.g., Terzaghi, 1965; Jing and Stephansson, 2007). That is, if those structures have a preferred orientation, their apparent number density along a scanline subparallel to this orientation is smaller than the true density. Numerical techniques have been developed to infer the unbiased orientation distribution for such cases (e.g., Mauldon et al., 2001; Peacock et al., 2003; Barthélémy et al., 2009).

Likewise, the observed orientation distribution of linear structures such as the axes of mesoscale slump folds is affected by selection bias. Here, mesoscale ones refer to such folds that their attitudes are observed in an outcrop. For example, folds with the axes perpendicular to an outcrop surface are easily discovered, but those parallel to the surface are not (Fig. 1). We do not observe the true but biased orientation distribution of such structures.

In this paper, we propose an inverse method to infer the unbiased distribution of the axes of slump folds. Such a technique is useful for basin analysis and for the understanding of soft-sediment deformations, because slump folds are often used to infer paleoslopes (e.g., Jones, 1939). The folds are thought to be formed during a reduction in velocity of slump sheets (e.g., Strachan and Alsop, 2006; Alsop and Holdsworth, 2007; Alsop and Marco, 2011), and therefore, are used to infer paleoslope directions. Folds are considered to dip upslope and to strike approximately normal to the slopes (Jones, 1939; Tucker, 2003; Bridge and Demicco, 2008). Hence, basin architecture has been inferred from their vergence (e.g., Woodcock, 1976; Bradley and Hanson, 1998; Noda and Toshimitsu, 2009). However, this popular view is known to have many exceptions (Hansen, 1971; La-

joie, 1972; Woodcock, 1979; Farrell, 1984; Strachan and Alsop, 2006; Debacker et al., 2009; Alsop and Marco, 2012).

To demonstrate our bias correction technique, we collected orientation data from the axes of mesoscale slump folds in the Cretaceous Izumi basin, Japan. The strata crop out along the Median Tectonic Line—the crustal-scale fault dividing the high-T and high-P metamorphic belts along the SW Japan arc (Miyashiro, 1961). The basin formation is attributed to the wrench tectonics along the fault (Ichikawa and Miyata, 1973) as a part of widespread wrench tectonics in Eastern Asia in the Cretaceous (Ren et al., 2002) driven by the oblique subduction of the Izanagi Plate (Taira et al., 1983; Maruyama et al., 1997). Miyata (1990) argue for wrench tectonics based on the observed cluster of the fold axis orientations. Accordingly, the slump folds of the Izumi Group are important for the understanding of the tectonic evolution of Japan and surrounding regions. The present technique was applied to slump folds to test if the popular view that the vergence and orientation of slump folds relates to paleoslope also holds true for structures in the Izumi Basin.

2. Method

2.1. Bias model

To construct a bias correction technique we considered, first, the way the orientation distribution was biased. The probability of the axis of a mesoscale fold to be exposed at an outcrop is comparable to Buffon's needle problem (e.g., Aigner and Ziegler, 2004, p. 135): What is the probability of a needle to lie across a line on a plane if the needle has a random orientation? A needle parallel to the line does not intersect the line, providing that the width of the needle is zero; whereas

the probability increases obviously with the angle made by the needle and the line. A needle perpendicular to the line has the maximum probability.

Probability is always defined to have a value between 0 and 1. Comparing the needle to an axis of mesoscale fold and the line to the surface of an outcrop (Fig. 2), it turns out that the probability of the axis to be exposed at the outcrop can be written as

$$|\boldsymbol{a} \cdot \boldsymbol{n}| = \cos\varphi, \tag{1}$$

where $\boldsymbol{a}$ is the unit vector representing fold axis, $\boldsymbol{n}$ is the unit vector normal to the outcrop surface and φ is the angle made by $\boldsymbol{a}$ and $\boldsymbol{n}$. This equation has a value between 0 and 1. The lengths of the folds were assumed to be independent from their orientations to regard Eq. (1) as the probability. In this work, we use this equation to model the selection bias for the observation of the mesoscale folds.

2.2. Forward model

We conducted Monte Carlo simulation to show the effect of the bias as follows. Slump folds were assumed to be embedded at various horizons of a sedimentary package with a homoclinal structure for simplicity. It was further assumed that the true orientation distribution of the fold axes had a clustered pattern with the central line on the bedding or had a girdle pattern on the bedding. Our bias correction aimed at inferring this pattern from the observed orientations of slump fold axes and from those of outcrops.

Both the clustered and girdle patterns are parameterized by the Bingham statistics (Love, 2007), the probability distribution of which has the maximum, intermediate and minimum concentration axes that are perpendicular to each other (Fig. 3). In addition, the distribution has the concentration parameters, κ_1 and κ_2

($\kappa_1 \leq \kappa_2 \leq 0$). The distribution has the probability density function,

$$F(\boldsymbol{x}) = \frac{1}{A} \exp\left[\boldsymbol{x}^{\top} \boldsymbol{Q}^{\top} \mathrm{diag}(\kappa_1, \kappa_2, 0)\, \boldsymbol{Q}\boldsymbol{x}\right],$$

where $\boldsymbol{x}$ is the unit column vector representing an orientation, A is the normalizing factor, $\boldsymbol{Q}$ is an orthogonal matrix representing the orientations of the axes. The absolute value, $|1/\kappa_1|$, stands for the spread of fold axes from the maximum to the minimum concentration axes, whereas $|1/\kappa_2|$ does from the maximum to the intermediate concentration axes. A girdle pattern, elliptical and circular clusters are represented by the parameters satisfying $\kappa_1 \ll \kappa_2 \approx 0$, $\kappa_1 \leq \kappa_2 \lesssim -10$ and $\kappa_1 = \kappa_2 \lesssim -10$, respectively.

We assumed that the maximum concentration axis lay on the bedding. It does not mean that fold hinges lay on the bedding. Instead, the hinges were assumed to be generally oblique to the bedding, and the spread of their orientations across the bedding is denoted by $|1/\kappa_1|$. The symbol, ψ, denotes the rake of the maximum concentration axis on the bedding (Fig. 4). The same symbol refers to the trend of the axis for horizontal bedding. In either case, ψ has a value between 0° and 180°. We dealt with slump folds in a homoclinal structure, but bedding attitudes had a variation to some extent. Variation of the angles made by the axes and the bedding is assumed, here, for dealing not only with the variation of the axes themselves but also that of the bedding attitudes in a largely homoclinal structure.

Observed orientation distribution of fold axes depends not only on the true distribution of the axes themselves but on the orientations of outcrop surfaces (Eq. 1). Fig. 5 shows the forward modeling of the bias using artificial data: the Bingham distribution with the parameters, $\kappa_1 = -10$ and $\kappa_2 = -1$, was assumed to be the true distribution (Fig. 5a). Horizontal bedding was assumed. Therefore, the trend of the maximum concentration axis is denoted by ψ. The stereogram in

Fig. 5b shows the poles to uniformly oriented 200 outcrop surfaces, whereas that in Fig. 5c shows the poles to N-S trending 200 cliffs where folds were assumed to be observed. Each of the poles is represented by the vector $\boldsymbol{n}$ in Eq. (1).

The observed orientation distributions for the cases of uniform and clustered orientations of outcrops were synthesized as follows. First, the unit vector, $\boldsymbol{a}$, representing a fold axis was generated thousands of times to make the Bingham distribution with $\kappa_1 = -10$ and $\kappa_2 = -1$ (Fig. 5a). Second, each of the times a uniform random number, p, between 0 and 1 was generated; and at the same time a vector $\boldsymbol{n}$ were randomly chosen from Fig. 5b or 5c. Third, the axis denoted by $\boldsymbol{a}$ was accepted if the vectors satisfy

$$\boldsymbol{a} \cdot \boldsymbol{n} > p. \tag{2}$$

Each of Figs. 5d and 5e shows the results with 10,000 accepted axes for the cases of Figs. 5b and 5c, respectively. The observed distribution resembles the true one if outcrops have random orientations (Fig. 5d). However, the peak density of the observed one is smaller than the true one, because fold axes subparallel to outcrop surfaces have non-zero probability to be observed. On the other hand, when the poles to outcrop surfaces were clustered, the synthesized orientation distribution of observed axes had a cluster similar to that of the outcrop poles (Fig. 5e), which was significantly different from the 'true' distribution.

2.3. Bias correction

Observed orientation distribution was unbiased by statistical inversion to determine the parameters, κ_1, κ_2 and ψ. Given the values of those parameters, the probability to discover a fold axis parallel to the unit vector $\boldsymbol{a}$ was calculated

through the procedure described in §2.2 (Fig. 5). Let $P(\boldsymbol{a}\,|\,\kappa_1, \kappa_2, \psi)$ be this probability. If $\boldsymbol{a}$ is regarded as a free variable, $P(\boldsymbol{a}\,|\,\kappa_1, \kappa_2, \psi)$ denotes the apparent or biased orientation distribution. Then, the similarity between the observed distribution and $P(\boldsymbol{a}\,|\,\kappa_1, \kappa_2, \psi)$ can be evaluated by the logarithmic likelihood function (e.g., van den Bos, 2007),

$$\mathcal{L}(\kappa_1, \kappa_2, \psi) = \sum_{i=1}^{N} \log P(\boldsymbol{a}^i\,|\,\kappa_1, \kappa_2, \psi),$$

where $\boldsymbol{a}^i$ is the unit vector parallel to the ith of N observed fold axes. Given the values of the triplet, ψ, κ_1 and κ_2, the left-hand side of this equation can be calculated from the observed directions, $\boldsymbol{a}^1$, $\boldsymbol{a}^2$, ..., $\boldsymbol{a}^N$. If $P(\boldsymbol{a}\,|\,\kappa_1, \kappa_2, \psi)$ had large values for those directions, the simulated distribution through the sampling bias was similar to the observed distribution. Therefore, the Bingham distribution with the triplet of parameter values that maximize $\mathcal{L}(\kappa_1, \kappa_2, \psi)$ was regarded as the most probable unbiased distribution of fold axes. The optimization of the parameters, κ_1, κ_2 and ψ, was conducted by the exhaustive search technique (e.g., Zabinsky, 2003).

The above method is tested with the artificial data in Fig. 5e. That is, a hundred orientations drawn from the distribution in the figure were assumed as the axes of observed folds, and we tested the method if it resulted in an unbiased distribution similar to the 'true' one in Fig. 5a. Fig. 6a shows the 100 orientations that were assumed to be observed axes of folds. Their maximum concentration axis had a NNW-SSE trend. They were unbiased using the orientations of outcrops in Fig. 5c. The grid search with the intervals of 0.5 for the concentration parameters and 15° for the trend of the axis resulted in the optimal values, $\hat{\kappa}_1 = -11.0$ and $\hat{\kappa}_2 = -1.5$, and the trend of 165° (Fig. 6c). The E-W trending maximum concentration

axis in Fig. 6a was clearly shown to be an artifact. The unbiased distribution (Fig. 6c) was similar to the 'true' one (Fig. 5a), which had the values, $\kappa_1 = -11$, $\kappa_2 = -1$ and $\psi = 0^\circ$. The low κ_2 value indicated that girdle patterns were favorable for the data. Therefore, unlike a dense and small cluster it was difficult to determine precisely the trend of the maximum concentration axis on the girdle.

3. Application to natural data

The bias correction technique was applied to mesoscale slump folds in the Cretaceous Izumi basin, SW Japan, to infer their true orientation distribution. We collected the orientation data along coasts to the south of Osaka, Japan (Fig. 7). Turbidites with a SE-dipping homoclinal structure cropped out along sea cliffs and on wave-cut platforms (Figs. 8, 9a).

Slump sheets and debris flow deposits were often intercalated in the turbidites (Tanaka, 1965). Groove and flute casts at the bases of turbidite beds evidence coherent west- to southwestward-directed paleocurrents (Fig. 7) (Miyata et al., 1987). South by southwestward paleocurrents were found in our study area (Fig. 9a)—southerly deflected from the west by southwestward regional average. Since the paleocurrent directions were determined from such sole marks that were observed excavated bedding planes, the orientation distribution of paleocurrents was free from the sampling bias that affected that of fold axes.

The succession shown in Fig. 9a was ~750 m in thickness—an apparent thickness because of the presence of outcrop-scale duplexes embedded in the succession. The slump folds that we measured the orientations of fold axes were not involved in the duplexes.

3.1. Observed slump folds

Slump sheets in the study area had thicknesses ranging from 0.3 to 2 m with the dominant thickness of ∼1 m. Sandstone layers in the sheets were typically 0.1 m in thickness with the maximum of 0.8 m, but were thickened or thinned or sometimes rifted during slumping. Slump sheets are thought to evolve into debris flows and eventually into turbidity currents (Strachan, 2008). We paid attention to such slump folds that sandstone beds in the folds were not disaggregated. The beds made asymmetric, tight–isoclinal folds: Isoclinal ones were usually recumbent (Fig. 10).

We observed slump fold axes along the coast (Fig. 9b). The axes made a cluster in the SE quadrant (Fig. 9c), roughly perpendicular to the southwestward paleocurrents (Fig. 9a). Therefore, the axes seem consistent with the classical view by Jones (1939). However, the vergences of the folds were bimodal with peaks in NE and SW quadrants (Fig. 9b), the former of which is inconsistent with the view. Fig. 9d is the histogram of the vergences, indicating the bimodal distribution. Miyata (1990) attributed the folding with northwestward vergences to pre-lithification gravity sliding by eastward tectonic tilting while the strata were soft.

However, we found that slump folds even in a slump sheet had various axial orientations (Fig. 11). The thicknesses of the sheet and the turbidite sandstone beneath it were measured along a coast, the location of which is shown in Fig. 7, for testing the correlation between the local undulations of the basin floor and the slump directions. The thickness of the sandstone had variations with an amplitude and wavelength of 10–20 cm and 20 m, respectively, suggesting a relatively smooth basin floor at the time of the slumping. In addition, the variations had no

systematic correlation with the slip directions.

Therefore, the applicability of the classical criteria to the slump folds to infer paleoslopes seems problematic. Since the dominant orientation of the fold axes were roughly perpendicular to the coast line (Fig. 9b), we suspected that the cluster of fold axes in the SE quadrant (Fig. 9c) was an artifact coming from sampling bias.

3.2. Inversion

The attitudes of outcrop surfaces were measured at 61 locations with the intervals of 70 m along the coast irrespective of the presence or absence of slump folds (Fig. 8). The poles to the outcrop surfaces had a cluster in the SE quadrant (Fig. 9e). The clustered orientations of the outcrops give rise to the apparent orientation distribution of the fold axes in favor of having a cluster in the same quadrant. On the other hand, the strata cropping out along the coast showed a homoclinal structure with the mean dip direction and dip was 154°/33°. We used this bedding attitude for the inversion.

The orientation distribution of the fold axes in Fig. 9c was unbiased with the orientations of outcrops in Fig. 9e. The exhaustive search with the intervals $\Delta\kappa_1 = \Delta\kappa_2 = 0.25$ and $\Delta\psi = 10^\circ$ resulted in the optimal values, $\hat{\kappa}_1 = -5.75$, $\hat{\kappa}_2 = -0.5$ and $\hat{\psi} = 50^\circ$. That is, the absolute value of $\hat{\kappa}_1$ was greater than that of $\hat{\kappa}_2$ by an order of magnitude. The corresponding Bingham distribution is shown in Fig. 9g, and the simulated distribution for the synthesized distribution of fold axes is shown in Fig. 9h.

The optimal values satisfy the condition, $\kappa_1 \ll \kappa_2 \approx 0$, indicating a girdle pattern of the unbiased distribution of fold axes. The minimum, intermediate and maximum concentration orientations of the unbiased orientation distribution had

the ratio of densities about 1:6:10. That is, our slump folds had largely random orientations on bedding planes with tendency to be clustered in the SW quadrant. The apparent orientation distribution had a cluster roughly in the same orientation, but the unbiased one had a lower peak density on the girdle compared to the apparent one (Fig. 9). The unbiased distribution was shown to have such a cluster, though the unbiased one was more girdle-like than the observed one.

The maximum concentration axis of the unbiased orientation was more or less perpendicular to the southwestward paleocurrents (Fig. 9), though the nearly girdle pattern of the unbiased distribution gave rise to a limited precision of the axis. Therefore, the popular view that the axes of slump folds are perpendicular to paleoslope applies to the folds in our study area in a statistical sense, but not necessarily to each of the folds. In addition, the hypothesis about the vergences of slump folds and paleoslope hold only about a half of the observed slump folds.

Strachan and Alsop (2006) noticed the relationship among fold axis, interlimb angle and paleoslope. That is, gentle and open folds had a tendency to have hinge lines perpendicular to paleoslope, and that tighter folds had random orientations because of the progressive rotations during folding. The slump folds in our study area showed this tendency: The hinges of gentle and open folds were perpendicular to the paleoslope that was indicated by paleocurrents (Fig. 12). In contrast, the folds with the angles smaller than $\sim 80^\circ$ had random orientations. However, this tendency may have been resulted also from the selection bias, because folds with large interlimb angles are discovered in an outcrop perpendicular to their hinge lines more easily than those in outcrops subparallel to the lines. Tight and isoclinal folds are readily recognized in outcrops, provided that their hinge zones are sectioned at the outcrops.

Miyata (1990) attributed the northeastward vergences of slump folds in the same area to post-burial and pre-lithification tectonic tilting resulting from the wrench tectonics along the Median Tectonic Line. The results of our study indicate that the slump folds do not evidence the tectonics. Alsop and Marco (in press) provide possible cause for the down-slope vergence of slump folds including the oscillatory currents induced by Tsunami. The sedimentological implications of the diverging vergences of slump folds is a matter of further studies in the Izumi basin.

4. Summary

Observation of the orientation distribution of mesoscale linear structures are affected by sampling bias, which comes from the angle made by the structures and an outcrop surface.

A numerical method to unbias the observed distribution using not only the observed one but also the orientations of outcrops.

The method was applied to the axes of mesoscale slump folds embedded in turbidites in the Cretaceous Izumi Group, SW Japan. Their apparent orientation distribution had a cluster in the SE quadrant. Their unbiased distribution had a girdle pattern with a maximum concentration axis in the same quadrant. The unbiased one had a lower peak density than the observed one.

The maximum concentration axis of the unbiased one was roughly perpendicular to the paleocurrents observed in the same area. Therefore, the popular view that the axes of slump folds are perpendicular to paleoslope applies to the folds in our study area in a statistical sense, but does not to each of the folds. In addition, the hypothesis about the vergences of slump folds and paleoslope hold only about

a half of the observed slump folds.

Acknowledgments

We thank Ian Alsop and an anonymous reviewer for helpful comments to improve the manuscript. Disussions with Hajime Naruse was fruitful. The stereonet software, Stereo32, written by Klaus Röller and Claudia Trepmann was used to draw some of the figures. This work was partly supported by the grant 21740364 from JSPS.

References

Aigner, M., Ziegler, G.M., 2004. Proofs from the Book, Third Edition. Springer, Berlin, 239pp.

Alsop, G.I., Holdsworth, R.E., 2007. Flow perturbation folding in shear zones. In: Ries A.C., Butler R.W.H., Graham R.D. (Eds.), Deformation of the Continental Crust: Geological Society, London, pp. 77–103.

Alsop, G.I., Marco, S., 2011. Soft-sediment deformation within seismogenic slumps of the Dead Sea Basin. Journal of Structural Geology 33 (4), 433–457.

Alsop, G.I., Marco, S., 2012. A large-scale radial pattern of seismogenic slumping towards the Dead Sea Basin. Journal of Geological Society 169 (1), 99–110.

Alsop, G.I., Marco, S., in press. Tsunami and seiche-triggered deformation within offshore sediments. Sedimentary Geology. doi:10.1016/J.sedgeo.2012.03.013.

Barthélémy, J.-F., Guiton, M.L.E., Daniel, J.-M., 2009. Estimates of fracture density and uncertainties from well data. International Journal of Rock Mechanics and Mining Sciences 46 (3), 590–603.

Bradley, D., Hanson, L., 1998. Paleoslope analysis of slump folds in the Devonian flysch of Maine. Journal of Geology 106 (3), 305–318.

Bridge, J.S., Demicco, R.V., 2008. Earth Surface Processes, Landforms and Sediment Deposits. Cambridge University Press, Cambridge, 815pp.

Debacker, T.N., Dunon, M., Matthys, A., 2009. Interpreting fold and fault geometries from within the lateral to oblique parts of slumps: A case study from the Anglo-Brabant Deformation Belt (Belgium). Journal of Structural Geology 31 (12), 1525–1539.

Farrell, S.G., 1984. A dislocationmodel applied to slump structures, Ainsa Basin, South Central Pyrenees. Journal of Structural Geology 6 (6), 727–736.

Fisher, N.I., Lewis, T., Embleton, B.J.J., 1993. Statistical Analysis of Spherical Data. Cambridge University Press, Cambridge, 329pp.

Hansen, E., 1971. Strain Facies. Springer-Verlag, Berlin, 207pp.

Ichikawa, K., Miyata, T., 1973. Pre-Miocene movements of the Median Tectonic Line. In: Sugiyama R. (Ed.), The Median Tectonic Line, Tokai University Press, Tokyo, pp. 87–95 [in Japanese].

Jing, L., Stephansson, O., 2007. The basics of fracture system characterization: Field mapping and stochastic simulations. Developments in Geotechnical Engineering 85, 147–177.

313 Jones, O.T., 1939. The geology of the Colwyn Bay district: A study of submarine slumping during the Salopian Period. Quarterly Journal of the Geological Society of London 95 (1–4), 335–382.

316 Kurimoto, C., Makimoto, H., Yoshida, F., Takahashi, Y., Komazawa, M., 1998. Map NI-53-15. Geological Map of Japan 1:200,000, Wakayama. Geological Survey of Japan, Tsukuba [in Japanese].

319 Lajoie, J., 1972. Slump fold axis orientations: An indication of paleoslope? Journal of Sedimentary Petrology 42 (3), 584–586.

321 Love, J.J. 2007. Bingham statistics. In: Gubbins D., Herrero-Bervira E. (Eds.), Encyclopedia of Geomagnetism and Paleomagnetism, Springer, Dordrecht, pp. 45–47.

324 Maruyama, S., Isozaki, Y., Kimura, G., Terabayashi, M., 1997. Paleogeographic maps of the Japanese Islands: Plate tectonic synthesis from 750 Ma to the present. Island Arc 6 (1), 121–142.

327 Mauldon, M., Dunne, W.M., Rohrbaugh, M.B., 2001. Circular scanlines and circular windows: New tools for characterizing the geometry of fracture traces. Journal of Structural Geology 23 (2–3), 247–258.

330 Miyashiro, A., 1961. Evolution of metamorphic belts. Journal of Petrology 2 (3), 277–311.

332 Miyata, T., 1990. Slump strain indicative of paleoslope in Cretaceous Izumi sedimentary basin along Median Tectonic Line, southwest Japan. Geology 18 (5), 392–394.

335 Miyata, T., Morozumi, Y., Shinohara, M., 1987. The Izumi belt. In: Nakazawa, K.,
336 Ichikawa K., Itihara M. (Eds.), Regional Geology of Japan 6, Kinki, Kyoritsu
337 Shuppan, Tokyo, pp. 60–65 [in Japanese].

338 Noda, A., Toshimitsu, S., 2009. Backward stacking of submarine channel-fan
339 successions controlled by strike-slip faulting: The Izumi Group (Cretaceous),
340 southwest Japan. Lithosphere 1 (1), 41–59.

341 Peacock, D.C.P., Harris, S.D., Mauldon, M., 2003. Use of curved scanlines and
342 boreholes to predict fracture frequencies. Journal of Structural Geology 25 (1),
343 109–119.

344 Ren, J., Tamaki, K., Li, S., Zhang, J., 2002. Late Mesozoic and Cenozoic rifting
345 and its dynamic setting in Eastern China and adjacent areas. Tectonophysics
346 344 (3–4), 175–205.

347 Strachan, L.J., 2008. Flow transformations in slumps: A case study from the Wait-
348 emata Basin, New Zealand. Sedimentology 55 (5), 1311–1332.

349 Strachan, L.J., Alsop, G.I., 2006. Slump folds as estimators of palaeoslope: A case
350 study from the Fisherstreet Slump of County Clare, Ireland. Basin Research 18
351 (4), 451–470.

352 Taira, A., Saito, Y., Hashimoto, M., 1983. The role of oblique subduction and
353 strike-slip tectonics in the evolution of Japan. In: Hilde T.W.C., Uyeda, S.
354 (Eds.), Geodynamics of the Western Pacific–Indonesian Region, American
355 Geophysical Union, Washington D.C., pp. 303–316.

Tanaka, K., 1965. Izumi Group in the central part of the Izumi Mountain Range, southwest Japan, with special reference to its sedimentary facies and cyclic sedimentation. Geological Survey of Japan Report 212, 1–34 [in Japanese].

Terzaghi, R.D., 1965. Sources of error in joint surveys. Geotéchnique 15 (3), 287–304.

Tucker, M.E., 2003. Sedimentary Rocks in the Field, Third Edition. Wiley, Chichester, 244pp.

van den Bos, A., 2007. Parameter Estimation for Scientists and Engineers. Wiley, Hoboken, 288pp.

Woodcock, N.H. 1976. Structural style in slump sheets: Ludlow Series, Powys, Wales. Journal of the Geological Society of London 132 (4), 399–415.

Woodcock, N.H. 1979. The use of slump structures as palaeoslope orientation estimators. Sedimentology 26 (1), 83–99.

Zabinsky, Z.B., 2003. Stochastic Adaptive Search for Global Optimization. Kluwer Academic, Boston, 224pp.

Fig. 1. The popular view about the shape of a slump fold and paleoslope: The latter is thought to be perpendicular to the fold axis and parallel to the vergence of the fold (e.g., Jones, 1939). Folds with the hinge lines perpendicular to an outcrop surface are discovered much more easily than those parallel to the surface.

Fig. 2. The hinge lines of slump folds (bold lines) in a rock body. The probability for a fold to be exposed depends on the angle, φ, made by the fold axis and the surface of an outcrop (dashed line).

Fig. 3. Equal-area projections showing the probability densities of Bingham distributions with different κ_1 and κ_2 values. Triangle, diamond and star depict the maximum, intermediate and minimum concentration axes of the distributions, respectively.

Fig. 4. Lower-hemisphere, equal-area projection showing an example of Bingham distribution to approximate the unbiased distribution of fold axes. The maximum, intermediate and minimum concentration orientations are indicated by triangle, diamond and star, respectively. The last one is perpendicular to bedding plane. The rake of the maximum concentration axis is denoted by ψ.

Fig. 5. Lower-hemisphere, equal-area projections showing the Monte Carlo simulation of the effect of the bias denoted by Eq. (1). (a) The contours of a Bingham distribution with the parameters, $\kappa_1 = -10$ and $\kappa_2 = -1$, with the N-S trending maximum concentration axis, for denoting the axes of mesoscale slump folds. (b, c) Poles to assumed 200 outcrop surfaces. (d, e) The contours of $P(\boldsymbol{a} \,|\, \kappa_1, \kappa_2, \psi)$.

That is, the orientation distributions of fold axes whose orientation data are expected to be collected from the outcrops. The distributions were synthesized from the true distribution (a) and the outcrop orientations (b, c). Triangle and star indicate the maximum and minimum concentration orientations, respectively.

Fig. 6. Lower-hemisphere, equal-area projections showing the bias correction applied to the artificial data in Fig. 5e. (a) A hundred orientations drawn from the data for representing observed fold axes. Triangle and star indicate the maximum and minimum concentration axes, respectively, determined through the orientation matrix of the data (Fisher et al., 1993). (b) Orientations representing the poles to the outcrop surfaces—the same data with Fig. 5c. (c) The Bingham distribution representing the orientation distribution of fold axes unbiased from (a). The distribution has the optimal values, $\hat{\kappa}_1 = -11.0$ and $\hat{\kappa}_2 = -1.5$, and the trend of the maximum concentration axis (triangle) at 165°. Star indicates the minimum concentration axis.

Fig. 7. Geologic map around the study area (Kurimoto et al., 1998) and paleocurrent directions of the Izumi Group (Miyata et al., 1987). The Median Tectonic Line is a crustal scale fault along the SW Japan arc.

Fig. 8. Outcrops in the study area, where the planar turbidite beds of the Cretaceous Izumi Group are exposed. The orientations of outcrops were measured at locations with intervals of 70 m along the coast.

Fig. 9. (a) Paleocurrents inferred from groove and flute casts. (b) Vergences of slump folds, the axes of which are perpendicular to the vergences. The lengths of arrows indicate the plunge angles. Tilt-corrections were not applied. (c–g) Lower-hemisphere, equal-area projections. Dotted lines depict the mean attitude of bedding. (c) Axes of mesoscale slump folds observed along the coast. Density contours were drawn by the software, Stereo32, using the cosine sum method with the cosine exponent at 20. (d) Histogram of the vergences, to which tilt-corrections were made. (e) Outcrop surfaces measured at locations with 70 m intervals along the coast. (f) Bedding planes observed on the coast. Cross denotes the mean. (g) Unbiased orientation distribution of fold axes determined from the data in (c) and (e). (h) Simulated orientation distribution of fold axes that are expected to be observed along the coast, i.e., the contours of $P(\boldsymbol{a} \mid \hat{\kappa}_1, \hat{\kappa}_2, \hat{\psi})$, where the parameters with accent marks denote the optimal values determined by the inversion. This distribution was synthesized from the data in (e) and the unbiased distribution in (g).

Fig. 10. A slump sheet in the study area. The lateral variations of the thicknesses of the sheet and underlying sandstone are shown in Fig. 11.

Fig. 11. Arrows indicate the vergences of folds in a slump sheet, and the lateral variations of the thicknesses of the sheet and its substratum (turbidite sandstone). A fold in the sheet with unclear vergence is depicted by a thin solid line perpendicular to the fold axis. The beds were exposed for a length of > 200 m along their strike. The location of this cliff is shown in Fig. 7.

445 **Fig. 12.** Polar plot showing the trends and interlimb angles of slump folds in the
446 study area. Most of folds with the angles greater than ~80° (highlighted by gray
447 lines) had hinges perpendicular to the general trend of paleocurrents (Fig. 9a).
448 Tilt correction was not applied to the trends.

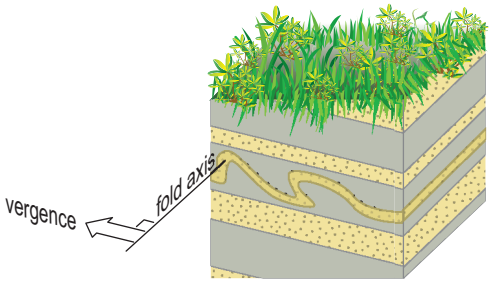

Figure 1:

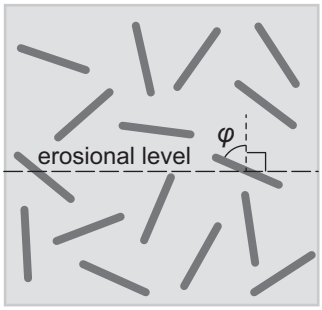

Figure 2:

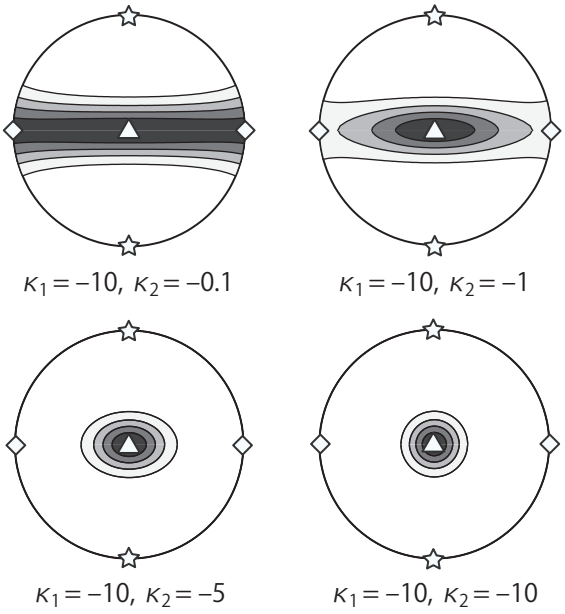

Figure 3:

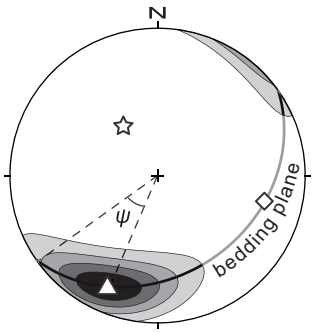

Figure 4:

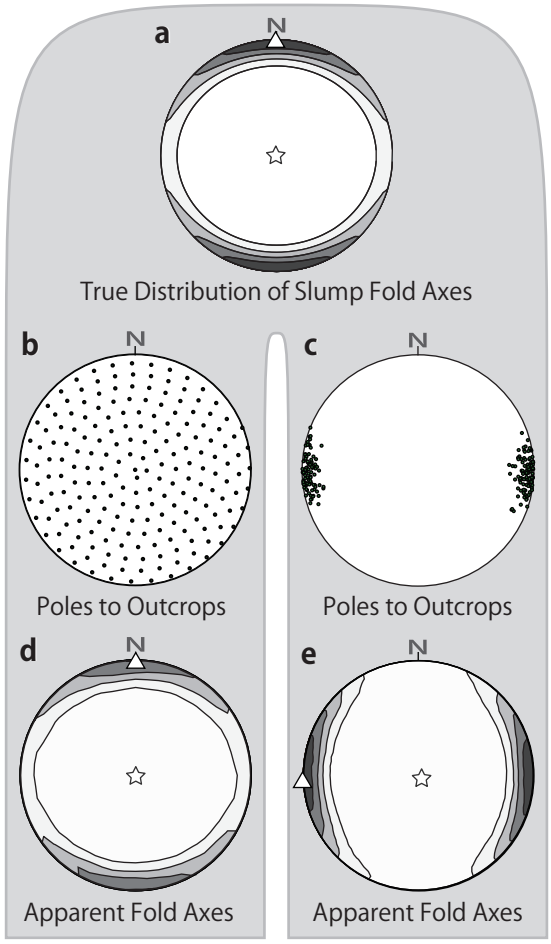
a
N
True Distribution of Slump Fold Axes
b
N
Poles to Outcrops
c
N
Poles to Outcrops
d
N
Apparent Fold Axes
e
N
Apparent Fold Axes

Figure 5:

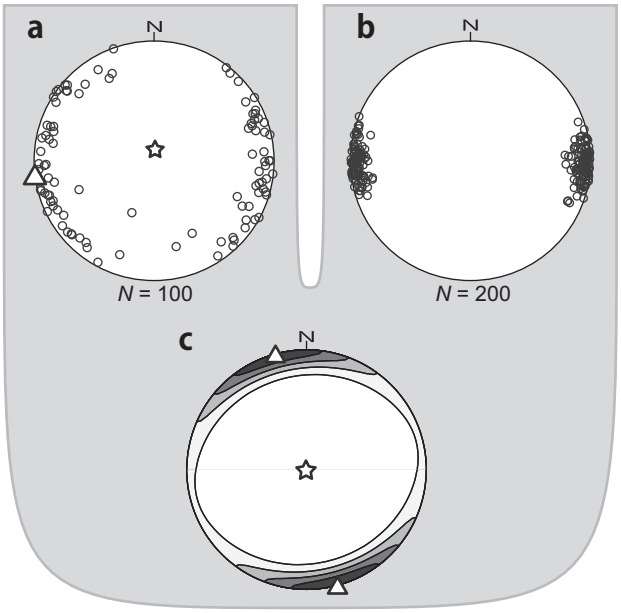

Figure 6:

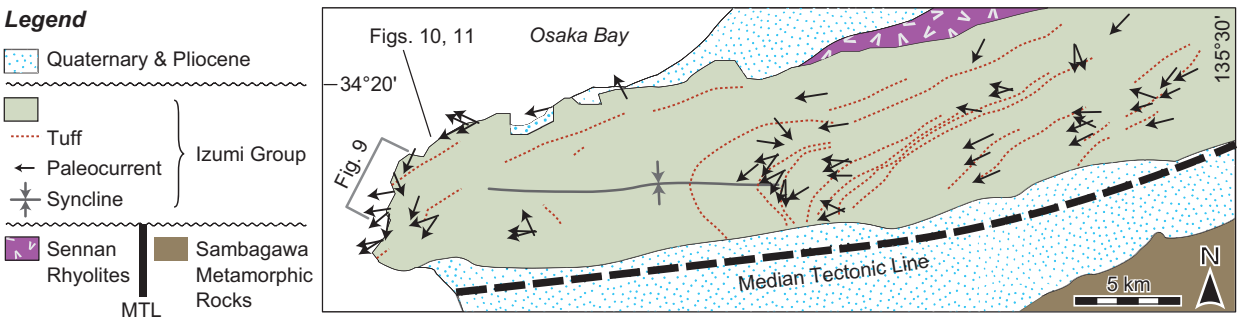

Figure 7:

Figure 8:

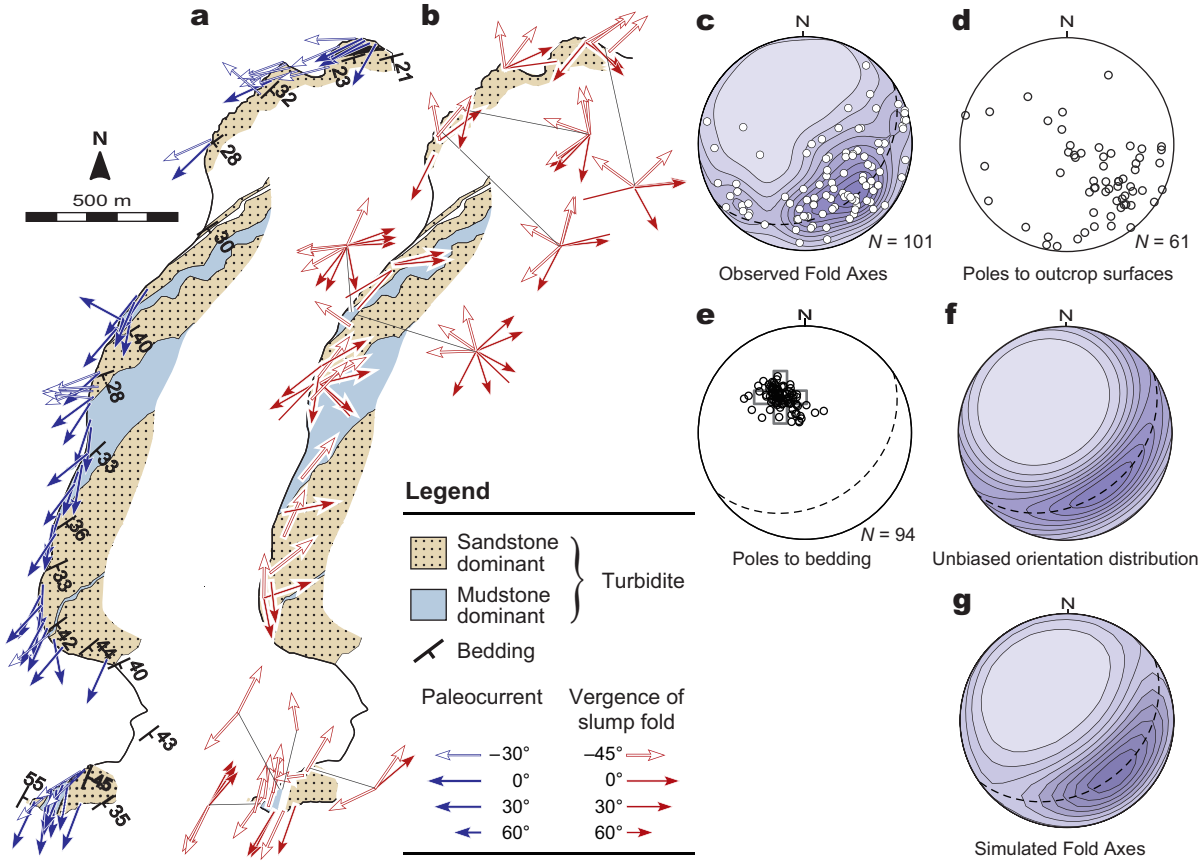
a
b
c
d
e
f
g
N
500 m
Legend
Sandstone dominant
Mudstone dominant
Turbidite
Bedding
Paleocurrent
Vergence of slump fold
−30°
0°
30°
60°
−45°
0°
30°
60°
N = 101
Observed Fold Axes
N = 61
Poles to outcrop surfaces
N = 94
Poles to bedding
Unbiased orientation distribution
Simulated Fold Axes

Figure 9:


Erosion Surface
Slump
Sheet
Sand-
stone
Fig : 11
50 cm
Basal Décollement

Figure 10:

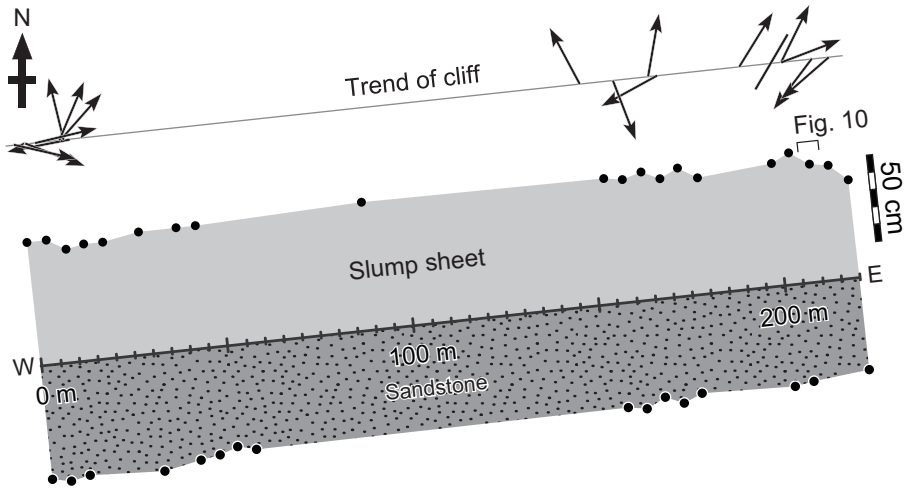
N
Trend of cliff
Fig. 10
50 cm
Slump sheet
E
200 m
100 m
W
0 m
Sandstone

Figure 11:

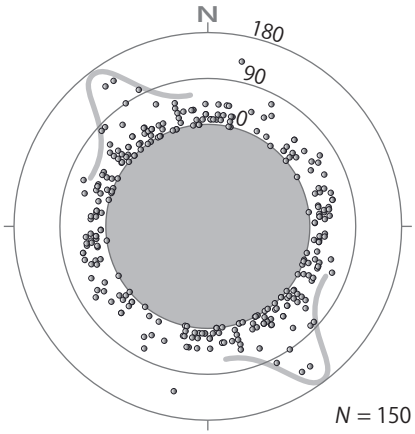

Figure 12: